EES Solar

PERSPECTIVE

View Article Online
View Journal | View Issue

Check for updates

Cite this: *EES Sol.*, 2025, **1**, 519

Additive engineering mechanisms in antimony chalcogenide solar cells: a focus on deeper understanding

Matthew Sutton [a] and Tayebeh Ameri *[abc]

Antimony chalcogenides represent a promising thin-film solar cell technology, offering inherently high stability, composed of elements more abundant than those used in established technologies such as CIGS and CdTe, and with the potential to approach the Shockley–Queisser efficiency limit of ~33%. However, the current efficiencies are low compared to the market leader, silicon, at around 10%. Chemical additives have been employed to achieve this efficiency, and many research groups believe they are key to achieving even higher efficiencies. However, to achieve that a keen focus on the mechanisms underlying the improvements gained from these additives is necessary, so upcoming research can build upon that prior work and more widely applicable knowledge in the field can be gained. In this article, we highlight some examples where the explanation/exploration of the mechanisms is done to an excellent degree. We hope that by highlighting these examples, steps will be taken towards more mechanism-focussed studies, which will yield more knowledge of the systems and behaviours present in antimony chalcogenide solar cells and the additives used to improve them.

Received 1st April 2025
Accepted 22nd July 2025

DOI: 10.1039/d5el00047e

rsc.li/EESSolar

Open Access Article. Published on 29 2025. Downloaded on 19.05.2026 16:14:10.
This article is licensed under a Creative Commons Attribution 3.0 Unported Licence.

Broader context

Antimony chalcogenide (Sb_2E_3, E = S, Se) solar cells are a promising technology that is comprised of earth abundant materials, has high inherent stability, a high absorption coefficient and a direct bandgap. The relative abundances of Sb, S and Se are greater than the rare elements in technologies such as CdTe, CIGS and GaAs, meaning that large-scale production can be more sustainably achieved with Sb_2E_3 than with those alternatives. Additionally, the inherent stability of these solar cells is a direct advantage over alternatives such as perovskites, which struggle with stability *vs.* moisture and air. As such, the advancement of this technology could lead to the development of a solar cell which is lightweight, stable and has a tuneable bandgap for use in outdoor and indoor environments, while also presenting opportunities to tandem with existing silicon technologies. Currently, the primary issue is that of low power conversion efficiency. By utilising chemical additives, the record efficiencies have reached 10.5, 10.7 and 10.75%, respectively. Thus, the investigation into and development of novel additives is of great importance for introducing Sb_2E_3 solar cells as a key player in the emerging solar materials field.

Introduction

It is widely recognized that excessive greenhouse gas emissions are a major driver of accelerated global climate change. In the US in 2022, electric power alone accounted for nearly a third of the emissions from fossil fuel combustion. Solar power is a renewable source of energy which involves the conversion of incoming solar radiation into useable electricity. It generates around one tenth of the equivalent greenhouse emissions per kWh compared to traditional fossil fuel technologies,[1] and so is a key technology alongside other renewable sources for reducing our overall emissions from the energy sector.

Crystalline silicon (c-Si) is the most mature and widely adopted solar cell material in the world to date, holding 95% of the market share in 2021.[2] This is attributed to high power conversion efficiency, excellent stability of approximately 30 years, and low costs, which have significantly declined over the past three decades. Notably, the global weighted average levelized cost of electricity for large PV systems dropped from €0.315 per kWh in 2010 to €0.047 per kWh in 2022.[3] However, due to an indirect bandgap, the film thickness has remained above 150 μm, with little to no decrease since 2006.[3] This increases the amount of material required and used for manufacture, and places c-Si in a poor position for lightweight applications such as electric vehicles. The silicon required, despite being earth-abundant, is also very energy intensive to refine into the pure silicon needed for solar cells, which reduces its effectiveness as a low-carbon energy source.[4] Thin film alternatives such as CIGS, CdTe and GaAs have a direct bandgap

[a]*Institute for Materials and Processes, School of Engineering, University of Edinburgh, Sanderson Building, Robert Stevenson Road, Edinburgh EH9 3FB, UK*
[b]*Chair for Composite Materials, Department of Materials Science, Faculty of Engineering, Christian-Albrechts-Universität zu Kiel, Kaiserstrasse 2, 24143 Kiel, Germany. E-mail: tam@tf.uni-kiel.de*
[c]*Kiel Nano, Surface and Interface Science KiNSIS, Kiel University, Christian-Albrechts-Platz 4, D-24118 Kiel, Germany*

© 2025 The Author(s). Published by the Royal Society of Chemistry

Open Access Article. Published on 29 2025. Downloaded on 19.05.2026 16:14:10.
This article is licensed under a Creative Commons Attribution 3.0 Unported Licence.

so can be made with thicknesses of 100s of nm and are already available at industrial scale. However, they are made from relatively scarce elements and contain highly toxic elements such as cadmium and arsenic, making them less suitable for mass production and widespread domestic use.[4] Another thin film technology, perovskites, have recently seen massive growth in the field, going from 14% to 26% efficiency in lab-scale in the last decade.[5] However, they suffer from inherent instability and contain toxic lead,[6] so again are less suitable for domestic applications. Various other thin film technologies such as organic solar cells are also available, though these also suffer from issues such as low stability, which limit their applications.[6]

Antimony chalcogenides (Sb_2E_3, E = S, Se) have significant potential to address many, if not all, of the issues mentioned above. They boast inherently high stability,[7–11] are formed of relatively abundant materials[7,9,11–16] through a variety of relatively low-energy deposition processes,[7,9,10,12–14,16–23] and have a strong absorption coefficient of $>10^5$ cm^{-1} at visible wavelengths.[7–16,24–26] The bandgap can also be tuned between 1.1 eV (Sb_2Se_3) and 1.8 eV (Sb_2S_3) through S/Se substitution, while retaining their orthorhombic crystal structure.[7–13,24–26] However, while it is theoretically possible to reach the Shockley–Queisser limit of ~32% using this bandgap tuning,[12] the highest efficiency reached to date is only 10.75%.[22] This is primarily due to deficient V_{OC} values that currently are only around half of their theoretical maxima, which are in turn due to the presence of defects in the crystal structure and band misalignment with the transporting layers.[24] Interface engineering and defect passivation are the primary ways to accomplish this, and a review on this topic was performed by Zhang *et al.* in 2021.[24] Practically, the most effective approach for accomplishing these tasks has involved the use of chemical additives such as ethylenediaminetetracetic acid (EDTA), NaF, and EtOH, which achieved efficiencies of 10.5%, 10.7%, and 10.75%, respectively.[22,25,27] However, the area in which antimony chalcogenides have the most promise is not in replacing c-Si, but in indoor applications, and in creating a stable tandem device with c-Si. The tuneable bandgap of 1.1–1.8 eV allows for the effective tuning for the optimal indoor bandgap of ~1.75 eV,[28] and the bandgap of 1.8 eV for Sb_2S_3 allows for the complementary absorption alongside the 1.12 eV bandgap of c-Si.[29]

However, despite these achievements, a deeper understanding of the processes involved in forming high-quality antimony chalcogenides, particularly the role of additives in this formation, is crucial for this solar technology to achieve the efficiencies required for placing this technology into the forefront of the solar research body.

Current understanding of additive engineering mechanisms

The primary challenge currently facing Sb_2E_3 solar cells is that of a low open circuit voltage (V_{OC}). A review on this topic was published in 2020 by Chao Chen and Jiang Tang,[30] and another by Yi Zhang *et al.* in 2021.[24] Chen and Tang highlight that while the short circuit current (J_{SC}) and fill factor (FF) in Sb_2E_3 solar cells have reached over 70% of the values predicted at the Shockley–Queisser limit (theoretical thermodynamic limit for single-junction solar cells), the open-circuit voltage (V_{OC}) of state-of-the-art cells is still less than 50%.[30] For comparison, crystalline silicon (c-Si) has surpassed 90% of its respective limit for J_{SC}, 80% for FF, and 90% for V_{OC}.[31] Therefore, to bring the overall performance of these cells to 15% and greater, minimizing the V_{OC} deficit is critical. Both reviews highlight two primary causes for this: interfacial recombination and defect-assisted recombination from deep-level trap states. Among various approaches, their suggestions to address these issues include: (i) passivation of defects from dangling bonds and mismatched lattices at the interfaces of Sb_2S_3, (ii) surface treatment of the ETL to enhance lattice matching or of Sb_2E_3 to reduce Sb_2O_3 formation, and (iii) p-type doping. Additionally, the growth of a highly crystalline, *hk*1-orientated absorber layer is of paramount importance for effective charge transportation and a high-performance solar cell.[12,13,17,18,25,32–38] Each of these effects can potentially be achieved through the use of chemical additives, and thus the understanding of chemical additives in Sb_2E_3 solar cells is a topic of great importance.

Additives have also been used effectively in other solar cell technologies, such as for passivating grain boundaries and interfaces in perovskite solar cells, where the established design rules allow for the relatively easy modification of many additives due to their organic nature.[39–42] If the desired functionality of an additive can be accurately determined, bespoke molecules can be synthesised which are optimised for the task at hand. Another good example of design rules being used to great effect is in organic solar cells, where even the absorbers themselves can be optimised and interchanged to maximise efficiency.[43] It is worth emphasising that this methodology is more suited to organic molecules due to the relative ease of altering their structures when compared to their inorganic counterparts.

Another key consideration with additive engineering is the method by which the additive will be applied. Unlike alternative technologies such as perovskite and organic solar cells, many of the synthesis methods for Sb_2E_3 require a high temperature post-annealing step,[7,12,20,25,27,44–46] which limits the use of most organic molecules for bulk-treatment purposes such as those seen for conjugated organic grain-boundary bridges in perovskite cells,[39–41] as organic compounds may decompose at the high temperatures required.[47] Similarly, when an additive is used to aid deposition, it is important to consider its potential presence in the final film, as this could introduce unwanted trap states and recombination centers. The different synthesis methods also vary in their compatibility with additives, particularly for bulk treatments of the absorber film. Hydrothermal (HT) and chemical bath deposition (CBD) have seen the most success.[7,12,20,25,44,46] As long as the additive is water-soluble, it can simply be added to the Sb_2E_3 reaction mixture prior to deposition. So, while other synthesis methods, such as vapour transport deposition and spray pyrolysis, offer benefits like growth on nanostructured substrates and high crystallinity,[16,19] they do not as readily accommodate the wide range of additives available for HT and CBD.

© 2025 The Author(s). Published by the Royal Society of Chemistry

Open Access Article. Published on 29 2025. Downloaded on 19.05.2026 16:14:10.
This article is licensed under a Creative Commons Attribution 3.0 Unported Licence.

Additives in Sb_2E_3 solar cells and their mechanisms

Achieving high performance is key to the success of antimony chalcogenides. They have high stability, varied and relatively low energy deposition processes and are made from abundant materials, but fall behind the competitors when it comes to performance. It is therefore essential to focus on this aspect when conducting research. However, we implore that this be accompanied by a drive to deeply understand the mechanisms which provide this performance, as this will serve to aid future research efforts and ultimately, yield more meaningful progress. This approach may also help prevent instances where the stability and/or benign nature of the material are compromised in favour of performance.

There are many different avenues through which additives can improve Sb_2E_3 solar cell performance, including defect passivation, improving lattice match, decreasing Sb_2O_3 formation, p-type doping of Sb_2E_3, and improved film crystallinity and orientation. Below, we detail various examples which make use of these effects. We highlight some excellent examples of where in-depth mechanistic investigation have yielded widely applicable and fundamental understanding, while also noting some examples where more in-depth mechanistic investigation would be beneficial to future works. The examples we highlight and discuss here are summarised in Table 1. Most of the 'overall effects' on the cell listed in Table 1 can be measured relatively easily using established techniques such as X-ray diffraction (XRD) and scanning electron microscopy (SEM). However, in many cases the details on how the additive achieves its effects are not fully explored. The majority of the listed additives function by reducing crystal defects and oxide phases. Therefore, by gaining a deeper understanding of the mechanisms underlying these effects, greater efficiency improvements beyond those already observed could be achieved.

To begin, we present a significant study conducted by the current leaders in Sb_2E_3 cell efficiency, Chen *et al.*, in which they used EtOH for a solvent-assisted hydrothermal deposition of $Sb_2(S,Se)_3$ and achieved 10.75%.[22] By observing the thickness and morphology of the films formed using various amounts of EtOH in the hydrothermal mixture, they found that EtOH has an effect on reaction kinetics. Specifically, it slowed the deposition of $Sb_2(S,Se)_3$, leading to an increase in crystallinity and crystal grain size. The key observation which led to this finding was that the film thickness was decreased in proportion to the amount of EtOH added. They proposed a potential explanation for the decrease in film thickness: the precursor potassium antimony tartrate (PAT) was less soluble in EtOH, thereby reducing the Sb available for deposition at any one time. Reducing the Sb available slowed down deposition and improved the crystallinity of the film, while also reducing the final thickness of the film since the overall reaction time remained constant. To prove their theory, they simply dissolved PAT and the other precursors in solutions of water, water/EtOH and EtOH, and saw a direct decrease in PAT solubility with increasing ratios of EtOH. The experiment clearly showing the effect of EtOH on the dissolution of the precursors PAT, sodium thiosulfate (STS) and selenourea (SU) is displayed in Fig. 1. This study provides solvent engineering as a direct and widely applicable method of lowering PAT solubility, leading to favourable film growth.

When EDTA was used by Wang *et al.* in 2020, they achieved a very high efficiency of 10.5%. However, their conclusion of the mechanism was based on a rational assumption that aggregates of the precursor potassium antimony tartrate exist and are broken up by EDTA.[25] While they explain their proposed mechanism clearly, they provide only improved crystal grain size and increased thickness in the final film as experimental evidence for this effect. Similarly, when PCDTBT was used in the recently published work of Mkawi *et al.*, they demonstrated an improvement in cell performance, through improved crystallinity and larger crystallite size.[51] While they conducted a thorough investigation of these superficial effects using XRD, Raman, SEM, and TEM, along with various PCDTBT concentrations, the role of PCDTBT was not explored experimentally, and the proposed mechanism remains unverified. We believe this highlights the challenges associated with the current emphasis on cell performance over mechanistic studies. For researchers aiming to build on the reported studies, there is limited practical information available, other than the observation that additives positively influenced the cell's performance by enhancing film quality.

A noteworthy illustration of a research endeavour that offers widespread and valuable insights into the underlying mechanisms is the work performed by Huang *et al.* in early 2022, with their chemical investigation into the hydrothermal process.[45] By scrutinizing the chemical properties of the hydrothermal deposition process of $Sb_2(S,Se)_3$, they were able to show that the altering the pH of the precursor solution can improve the film deposition. To determine this, they utilised pH measurements, thermogravimetric analysis (TGA), scanning electron microscopy energy-dispersive X-ray spectroscopy (SEM-EDS) and a simple but effective method of trapping volatiles using an upturned funnel. They also analysed the film for defects using deep-level transient spectroscopy (DLTS). The results of these experiments can be seen in Fig. 2. They found that during the annealing process, sulfur and selenium escape from the film, forming pinholes and reducing solar cell performance. To remedy this, they proposed that under acidic conditions, an intermediate phase $Sb_2(S_x,Se_y)_3$, where $x + y > 1$, forms, which leads to release of S and Se and the formation of pinholes. Therefore, by increasing the pH, these pinholes could be effectively suppressed. However, one of the precursors, $Na_2S_2O_3$, was particularly sensitive to pH. To address these constraints while avoiding the introduction of additional impurities from conventionally used bases, they incorporated an H^+-selective zeolite into the solution, which improved the efficiency from 7.28% to 8.87%. This bottom-up approach enabled them to identify potential issues with other additives and address them prior to testing in complete devices.

Another study which made good use of already existing widespread knowledge on the underlying mechanisms was conducted by Huang *et al.* in early 2023, exploring

Open Access Article. Published on 29 2025. Downloaded on 19.05.2026 16:14:10.
This article is licensed under a Creative Commons Attribution 3.0 Unported Licence.

Table 1 Examples of chemical additives and their overall effects in Sb_2E_3 solar cells. Performance of the standard device is reported in brackets

Additive and solar cell information					Performance					
Additive	Application method	Sb_2E_3 system	Synthesis method	Overall effect on cells	V_{OC} (V) [standard]	J_{SC} (mA cm^{-2}) [standard]	FF [standard]	Efficiency (%) [standard]	Efficiency improvement (%)	Ref.
Ethanol	Bulk	S/Se	HT	Limits availability of Sb	0.63 [0.65]	25.3 [22.2]	0.67 [0.63]	10.8 [9.12]	17.8	22
Ethylenediaminetetraacetic acid (EDTA)	Bulk	S/Se	HT	Improved crystallinity	0.66 [0.61]	23.8 [23.3]	0.66 [0.66]	10.5 [9.40]	11.7	25
NH_4F	Bulk	S/Se	HT	Dissolution and redeposition of CdS electron transfer layer	0.63 [0.62]	24.8 [22.7]	0.66 [0.65]	10.28 [9.16]	12.2	46
Zeolite	Bulk	S/Se	HT	Reduced defects and oxide phases	0.57 [0.57]	23.6 [20.6]	0.66 [0.62]	8.87 [7.28]	21.8	45
Thioacetamide (+thiourea)	Bulk	S	CBD	Reduced defects and oxide phases	0.76 [0.73]	17.4 [15.9]	0.60 [0.56]	8.00 [6.49]	23.3	44
$N(NH_4)_2S$	Bulk	S	HT	Reduced defects and oxide phases	0.76 [0.78]	15.8 [13.8]	0.58 [0.56]	6.92 [6.01]	15.1	48
[TMA][PF_6]	Bulk	S	Spin coated	Limits availability of Sb	0.66 [0.58]	17.7 [14.9]	0.59 [0.51]	6.83 [4.43]	54.2	49
Tartaric acid	Bulk	S	HT	Reduced defects and oxide phases	0.75 [0.74]	14.1 [12.9]	0.59 [0.57]	6.31 [5.46]	15.6	50
4-Chloro-3-nitrobenzenesulfonyl chloride	Bulk	S	Spin coated	Limits availability of Sb	0.62 [0.58]	15.9 [13.8]	0.60 [0.52]	5.84 [4.20]	39.0	36
PCDTBT	Bulk	S	HT	Improved crystallinity	0.47 [0.42]	16.5 [9.94]	0.67 [0.63]	5.11 [2.61]	95.8	51
Phosphotungstic acid	Bulk	S	CBD	Suppression of oxides and oxyhalides	0.69 [0.57]	13.3 [8.57]	0.49 [0.39]	4.61 [1.91]	141	52
NaF (KF, RbF, CsF)	Post-treatment	S/Se	HT	Improved band alignment	0.67 [0.66]	23.7 [22.2]	0.67 [0.63]	10.7 [9.20]	16.3	27
$SbCl_3$	Post-treatment	S	Spin coated	Reduced defects and oxide phases	0.72 [0.58]	17.2 [14.7]	0.57 [0.51]	7.10 [4.37]	62.5	53
Thioacetamide	Post-treatment	S	CBD	Reduced surface defects and oxide phases	0.65 [0.57]	16.7 [15.2]	0.65 [0.64]	7.10 [5.50]	29.1	20
H_2S	Post-treatment	S/Se	Thermal evaporation	Reduced defects and oxide phases	0.38 [0.35]	27.9 [18.6]	0.56 [0.46]	5.98 [3.08]	94.2	23
KSCN/LiSCN	Post-treatment	S	CBD	Doping of CuSCN hole transport layer	0.49 [N/A]	14.1 [N/A]	0.49 [N/A]	3.37 [N/A]	N/A	54 and 55

© 2025 The Author(s). Published by the Royal Society of Chemistry

Open Access Article. Published on 29 2025. Downloaded on 19.05.2026 16:14:10.
This article is licensed under a Creative Commons Attribution 3.0 Unported Licence.

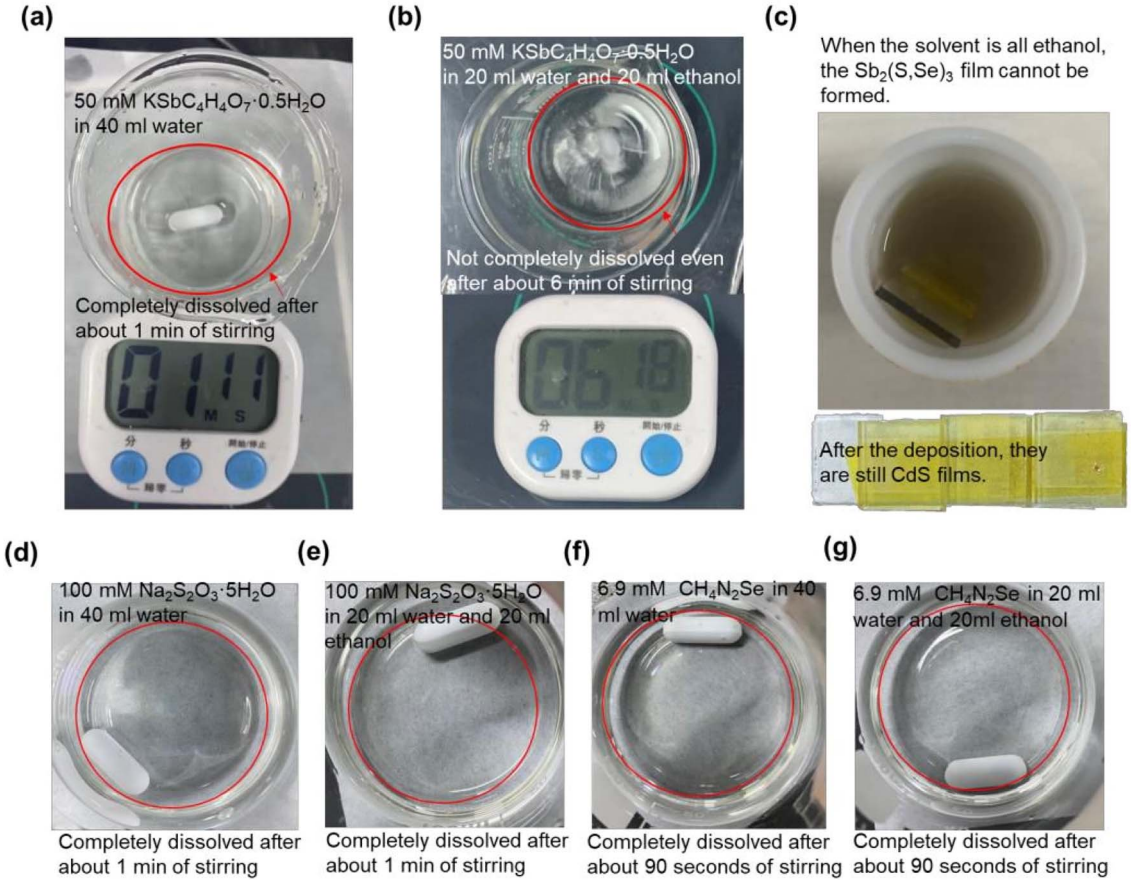

Fig. 1 Dissolution process of the same amount of $KSbC_4H_4O_7 \cdot 0.5H_2O$ (PAT), $Na_2S_2O_3 \cdot 5H_2O$ (STS) and CH_4N_2Se (SU). (a) PAT in deionized water for stirring about 1 min and (b) PAT in deionized water/ethanol mixed solvents for stirring about 6 min at the same speed. After stirring, PAT was completely dissolved in deionized water, but not in deionized water/ethanol mixture. (c) When deionized water is totally replaced by ethanol, the $Sb_2(S,Se)_3$ film cannot be formed. (d) STS in deionized water, (e) STS in deionized water/ethanol mixed solvents, (f) SU in deionized water, (g) SU in deionized water/ethanol mixed solvents. The STS and SU can be totally dissolved both in water and water/ethanol mixed solvents for stirring with 2 minutes. Reproduced from ref. 22 with permission from Wiley, copyright 2023.

a hydrothermal sulfurization strategy.[48] Sulfurization is a well-established method for enhancing antimony sulfide films through the reduction of S vacancies and oxide phases.[23,44,45,48,50] They described their sulfurization mechanism involving $(NH_4)_2S$ as the formation of NH_3 and H_2S during the hydrothermal process, driven by a well-known hydrolysis reaction. These processes were combined to give an effective hot *in situ* sulfur source in the form of H_2S during deposition. While they explain that the H_2S provided S atoms to fill sulfur vacancies, they do not discuss their observed reduction of oxide phases. This likely occurred due to the reaction of H_2S with oxide impurities, thereby removing the oxides and forming antimony sulfide and water. In the end, they improved the efficiency from 6.01% to 6.92%.

Studies often build on insights from other solar technologies, where much of the mechanistic explanation may already be established. However, it remains crucial to elucidate the role of the additive within the context of the new field or system. For example, when Zhao *et al.* attained 10.7% in $Sb_2(S,Se)_3$ cells through the use of NaF in 2021, they based their work on prior successful experiments on $Cu(In,Ga)Se_2$ (CIGS) solar cells.[56,57] However, they importantly still investigated the new system and found that the NaF etches sulfur from the film, thereby decreasing the S/Se gradient and leading to more favourable band alignment in the solar cell. In this case, they had ample experimental evidence for this gradient and its decrease in the form of energy-dispersive X-ray spectroscopy (EDS), secondary ion mass spectroscopy (SIMS) and a shift in powder X-ray diffraction (PXRD) peaks, shown in Fig. 3.[27] SIMS showed that the S/Se grading was decreased after solution post-treatment (SPT) with alkali metal fluorides, leading to a more spatially flat valence band maximum, and thus improved charge injection from the HTL. They also measured the sodium and fluorine concentration at various points in the films using SIMS and concluded that sodium doping was likely a key factor in the improved performance. However, uncovering the specific reasoning behind what was causing the grading effect could pave the way for the future discovery or design of a reagent that performs this function even more effectively. They hint at a potential mechanism by stating that "We speculate that this change of S/Se grading may be caused by the etching of weakly alkaline NaF aqueous solution". They go on to explain that this

Open Access Article. Published on 29 2025. Downloaded on 19.05.2026 16:14:10.
This article is licensed under a Creative Commons Attribution 3.0 Unported Licence.

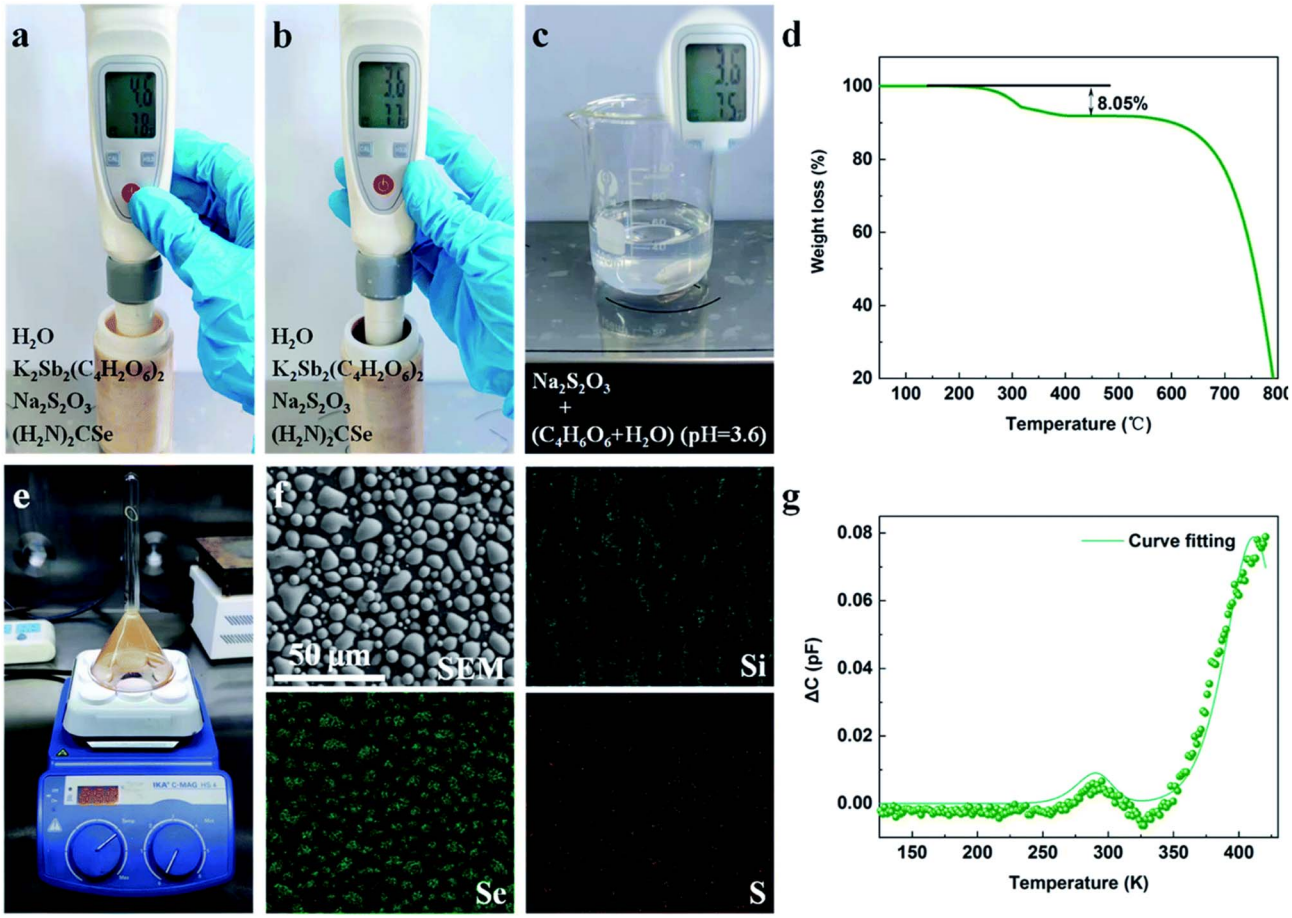

Fig. 2 The pH values of solutions before (a) and after (b) hydrothermal reaction, and the photo of the solid $Na_2S_2O_3$ dissolved in $C_4H_6O_6$ solution at a pH value of 3.6 (c). (d) TGA curve of the as-prepared $Sb_2(S,Se)_3$ powder. (e) The photo of the as-prepared $Sb_2(S,Se)_3$ powder annealed at 350 °C for 10 min. (f) The SEM image and EDS-mapping of volatiles in (e). (g) DLTS signals of the as-prepared $Sb_2(S,Se)_3$ device. Reproduced from ref. 45 with permission from Royal Society of Chemistry, copyright 2022.

etching was likely selective towards Se, and thus caused a decrease in the overall S/Se grading of the film. Ideally, a control experiment would have been conducted in order to isolate and confirm this effect, such as placing a sample produced with intentional S/Se grading into aqueous NaF for an extended period followed by measurement in SIMS.

Another study which made use of additives established in other solar technologies was the study of phosphotungstic and related heteropoly acids by Chen *et al.* in 2018.[52] Heteropoly acids are known for their use in dye-sensitised solar cells for enhancement of the injection and transport of electrons into and within the TiO_2 photoanode, and broadening of the absorption spectrum in the visible region.[58] In the study on the effects of heteropoly acids as additives in Sb_2S_3 cells, the cell efficiency was improved from 1.91% without any additive to 4.49% by using phosphotungstic acid. Using SEM, they observed that the phosphotungstic acid cells had fewer pinholes than the standard and concluded that this likely led to the large J_{SC} increase, ultimately increasing the overall efficiency. They conducted a mechanistic investigation of various heteropoly acids and concluded, based on a comparison of their acidity and oxidative potentials, that high acidity and low oxidative potential are essential for an effective additive in Sb_2S_3 solar cells. However, they compare these properties only within heteropoly acids and not with other acids, aside from HCl. While they note that HCl may have a positive impact on performance, they also highlight its potential to damage the final Sb_2S_3 film. Additionally, they did not propose or demonstrate a detailed chemical mechanism for how acidity or oxidative potentials suppress Sb_2O_3, which limits the broader applicability of their findings for designing new additives.

We aimed to embody the ideals laid out in this article in our latest work, in which we investigated the mechanisms underlying the functionality of the established EDTA additive.[59] Using NMR spectroscopy, we provided evidence of the proposed working mechanism of EDTA in Sb_2E_3 solar cells, whereby EDTA binds to Sb^{3+} in solution and reduces its availability for deposition. Additionally, we discovered a screening process that led to the identification of several other effective additives. This screening process involved making a solution of the precursors PAT and STS, then adding the additive to be tested. The solution was then left in ambient conditions over a day, and the resultant

© 2025 The Author(s). Published by the Royal Society of Chemistry

Open Access Article. Published on 29 2025. Downloaded on 19.05.2026 16:14:10.
This article is licensed under a Creative Commons Attribution 3.0 Unported Licence.

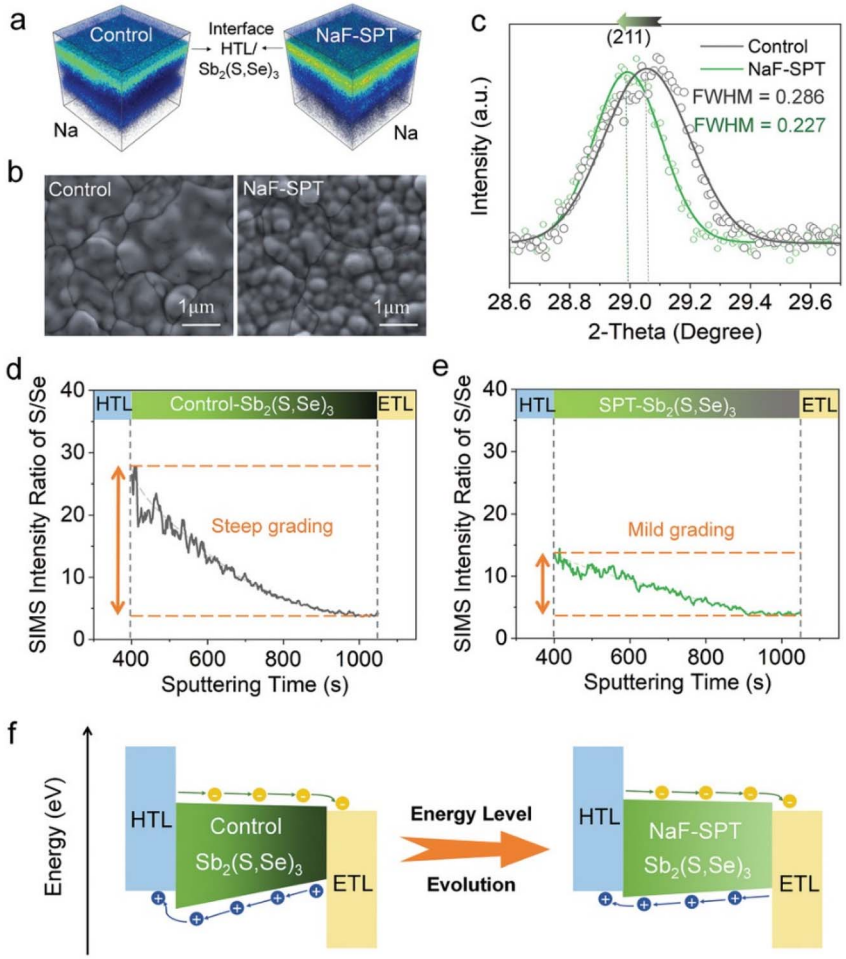

Fig. 3 (a) 3D-SIMS images of Na. (b) Surface SEM images. (c) Enlarged XRD spectra of 2-theta from 28.6° to 29.8°. (d and e) SIMS intensity ratios of S/Se in $Sb_2(S,Se)_3$ films. (f) Schematic diagram of energy levels of $Sb_2(S,Se)_3$ devices with or without NaF-SPT. Reproduced with from ref. 27 with permission from Wiley, copyright 2022.

precipitation indicated the viability of an additive, and if any unwanted side-reactions were present. The most performant additives formed a red precipitate, which we found to be amorphous Sb_2S_3, and the least performant formed a white precipitate, which we found to be Sb_2O_3. An example of solutions with and without EDTA and their resultant powders can be seen in Fig. 4.

Ultimately, we presented a generally applicable methodology for preventing the formation of Sb_2O_3 in antimony chalcogenide solar cells through pH control. The performances of the

Fig. 4 Vials of Sb_2S_3 precursors sodium thiosulfate (STS) and potassium antimony tartrate (PAT) in water (left), and EDTA + STS + PAT in water (right), showing that upon addition of EDTA, a red powder forms over time in ambient conditions. Reproduced from ref. 59 with permission from Royal Society of Chemistry, copyright 2025.

Open Access Article. Published on 29 2025. Downloaded on 19.05.2026 16:14:10.
This article is licensed under a Creative Commons Attribution 3.0 Unported Licence.

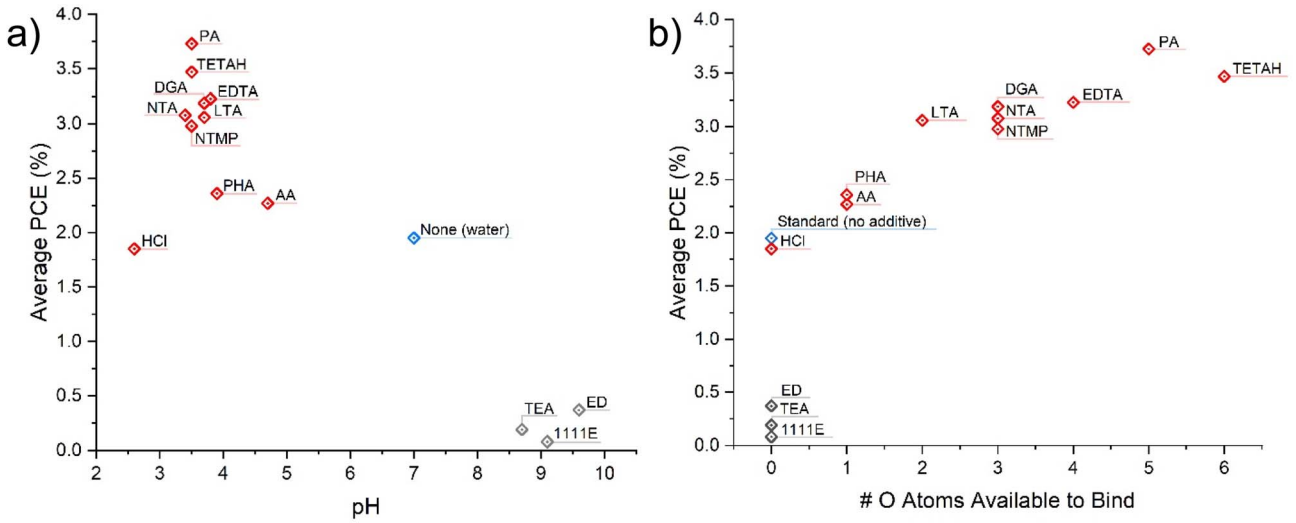

Fig. 5 Correlation of (a) the pH and (b) the number of potential Sb-binding O atoms of an additive employed in Sb_2S_3 solar cells, and the performance of that additive in a solar cell. The additives used were none (standard), ethylenediaminetetraacetic acid (EDTA), pentetic acid (PA), triethylenetetramine-*N*,*N*,*N*′,*N*″,*N*‴,*N*‴-hexaacetic acid (TETAH), nitrilotriacetic acid (NTA), diglycolic acid (DGA), L-(+)-tartaric acid (LTA), nitrilotris(methylenephosphonic) acid (NTMP), phosphoric acid (PHA), acetic acid (AA), hydrochloric acid (HCl), triethanolamine (TEA), ethylenediamine (ED) and 1,1′,1″,1‴-(ethane-1,2-diylbis(azanetriyl))tetrakis(propan-2-ol) (1111E). Reproduced from ref. 59 with permission from Royal Society of Chemistry, copyright 2025.

additives were correlated with their pH, and with their potential for binding to Sb^{3+}. The results of these correlations are shown in Fig. 5. We showed that by decreasing the pH of the solution, Sb_2O_3 can be effectively suppressed, leading to improved efficiencies. In our publication, we proposed suitable mechanisms for this occurring through the conversion of Sb_2O_3 to Sb_2S_3. In addition, our proposed mechanisms also further explained the Sb_2O_3 suppressive properties observed by Chen *et al.* for phosphotungstic acid.[52] In our work, while lowering the pH suppressed the formation of Sb_2O_3, a side reaction leading to elemental sulfur occurred at pH levels below 3. Thus, the optimal pH was determined to be approximately 3.6. Additionally, the ability of an additive to bind Sb^{3+} strongly correlated with its performance, providing an explanation for the observed discrepancies among acidic additives. This binding likely plays a more critical role once Sb_2O_3 formation is suppressed. By binding Sb^{3+} in solution, the additive reduces the free Sb concentration, effectively controlling deposition, enhancing film crystallinity, and improving solar cell performance.

Importantly, by starting with an in-depth investigation of an established additive, we provided a generally applicable and fundamental understanding that can be directly applied to the development of new additives, while also helping to further explain the observed effects of already established additives.

Conclusions and outlook

The field of antimony chalcogenides has rapidly advanced in the past decade, and the future of the field looks highly promising. However, for this advancement to continue apace, vigilance must be taken to ensure progress is accompanied by understanding of the reasons behind said progress. Improvement of cell performance without a clear, experimentally validated explanation is of little use to the wider research body and can even mislead future studies if incorrect assumptions are made. To contribute more valuable insights to the broader research community and facilitate advancements in antimony chalcogenide solar cells, our suggestion is to shift our attention towards understanding the underlying factors driving performance enhancements. By prioritising the exploration of the reasons behind the performance improvements, progress will naturally follow as our comprehension deepens. This deeper understanding will also naturally aid newer researchers in the field with concrete, validated evidence and explanations of underlying principles on which they can base their work, further aiding the drive towards high-efficiency cells. Gaining this understanding is often very challenging, but we hope that by highlighting some examples where excellent investigation has been performed, we can inspire more novel approaches to be developed. We highlighted examples of what has been achieved to date in the field of antimony chalcogenide additive engineering, most notably:

- Improvement in film quality *via* the reduction of the availability of Sb^{3+} in the hydrothermal deposition solution, achieved either by the reduction of Sb^{3+} solubility with ethanol, or the chelation of Sb^{3+} using EDTA and similar additives.
- The reduction of S and Sb vacancies by various chemicals, such as H_2S, $SbCl_3$ and thioacetamide in bulk and surface treatments.
- The control of the chemical environment and pH, using zeolites and various acidic additives to suppress and convert oxide phases to sulfide phases.

One aspect which is still unclear is why the reduction of antimony solubility is beneficial to the film deposition, and how it may be better controlled by using alternative Sb sources.

© 2025 The Author(s). Published by the Royal Society of Chemistry

Open Access Article. Published on 29 2025. Downloaded on 19.05.2026 16:14:10.
This article is licensed under a Creative Commons Attribution 3.0 Unported Licence.

Additionally, the way in which additives incorporate into the film (particularly considering the relatively high temperature annealing step of approximately 300–400 °C) is as yet unknown and is of great importance for understanding the formation and suppression of S and Sb defects in the film. The effects of pH are also dependent on the deposition system being employed, so while in our study we covered the effects of pH in the most commonly used hydrothermal STS/PAT system, other systems would likely benefit from similar study. Future works should seek to tackle these outstanding issues, so that we may have a more complete understanding of the working mechanisms of the additives we employ.

We believe a greater focus on mechanisms and processes involved in the formation of good quality antimony chalcogenide solar cells is paramount to continued progress and to encourage new researchers and academics to join this exciting field. With a clear and in-depth understanding, the design and development of high-performance, environmentally benign, and low-cost additives will become both easier and faster.

Data availability

No primary research results, software or code have been included and no new data were generated or analysed as part of this review.

Conflicts of interest

There are no conflicts to declare.

Acknowledgements

T. A. acknowledges finance support of DFG Heisenberg Programme, project AM 519/4-1.

References

1 M. Pehl, A. Arvesen, F. Humpenöder, A. Popp, E. G. Hertwich and G. Luderer, *Nat. Energy*, 2017, **2**, 939–945.
2 *Special Report on Solar PV Global Supply Chains*, IEA, 2022.
3 *Photovoltaics Report*, Fraunhofer Institute for Solar Energy Systems, 2024, **https://www.ise.fraunhofer.de**.
4 M. E. I. Rader Jensen, Efficient Utilization of Elements, *The Chemical Sciences and Society Summit*, Narita, Japan, 2013.
5 *Best Research-Cell Efficiency Chart*, National Renewable Energy Laboratory, **https://www.nrel.gov/pv/cell-efficiency.html**, 2024.
6 M. Heinrich, T. Kuhn, F. Dimroth, U. Würfel, J. C. Goldschmidt, M. Powalla, S. W. Glunz and D. H. Neuhaus, A Comparison of Different Solar Cell Technologies for Integrated Photovoltaics, presented in *Part at the 37th European PV Solar Energy Conference and Exhibition*, Lisbon Congress Centre, 2020.
7 C. Jiang, J. Zhou, R. Tang, W. Lian, X. Wang, X. Lei, H. Zeng, C. Zhu, W. Tang and T. Chen, *Energy Environ. Sci.*, 2021, **14**, 359–364.
8 C. Wu, L. Zhang, H. Ding, H. Ju, X. Jin, X. Wang, C. Zhu and T. Chen, *Sol. Energy Mater. Sol. Cells*, 2018, **183**, 52–58.
9 C. Wu, W. Lian, L. Zhang, H. Ding, C. Jiang, Y. Ma, W. Han, Y. Li, J. Zhu, T. Chen and C. Zhu, *Sol. RRL*, 2020, **4**, 1900582.
10 S. Fan, C. Shi, K. Lv, Q. Wang, F. Guo and W. Chen, *J. Nanopart. Res.*, 2021, **23**, 42.
11 C. Wu, C. Jiang, X. Wang, H. Ding, H. Ju, L. Zhang, T. Chen and C. Zhu, *ACS Appl. Mater. Interfaces*, 2019, **11**, 3207–3213.
12 R. Tang, X. Wang, W. Lian, J. Huang, Q. Wei, M. Huang, Y. Yin, C. Jiang, S. Yang, G. Xing, S. Chen, C. Zhu, X. Hao, M. A. Green and T. Chen, *Nat. Energy*, 2020, **5**, 587–595.
13 Y. Yin, C. Jiang, Y. Ma, R. Tang, X. Wang, L. Zhang, Z. Li, C. Zhu and T. Chen, *Adv. Mater.*, 2021, **33**, 2006689.
14 L. Wang, D.-B. Li, K. Li, C. Chen, H.-X. Deng, L. Gao, Y. Zhao, F. Jiang, L. Li, F. Huang, Y. He, H. Song, G. Niu and J. Tang, *Nat. Energy*, 2017, **2**, 17046.
15 M. M. Nicolás-Marín, F. Ayala-Mato, O. Vigil-Galán and M. Courel, *Sol. Energy*, 2021, **224**, 245–252.
16 Y. Pan, X. Hu, Y. Guo, X. Pan, F. Zhao, G. Weng, J. Tao, C. Zhao, J. Jiang, S. Chen, P. Yang and J. Chu, *Adv. Funct. Mater.*, 2021, **31**, 2101476.
17 L. Zhang, W. Lian, X. Zhao, Y. Yin, T. Chen and C. Zhu, *ACS Appl. Energy Mater.*, 2020, **3**, 12417–12422.
18 C. Chen, Y. Yin, W. Lian, L. Jiang, R. Tang, C. Jiang, C. Wu, D. Gao, X. Wang, F. Fang, C. Zhu and T. Chen, *Appl. Phys. Lett.*, 2020, **116**, 133901.
19 R. Parize, A. Katerski, I. Gromyko, L. Rapenne, H. Roussel, E. Kärber, E. Appert, M. Krunks and V. Consonni, *J. Phys. Chem. C*, 2017, **121**, 9672–9680.
20 Y. C. Choi, D. U. Lee, J. H. Noh, E. K. Kim and S. I. Seok, *Adv. Funct. Mater.*, 2014, **24**, 3587–3592.
21 H. Deng, Y. Zeng, M. Ishaq, S. Yuan, H. Zhang, X. Yang, M. Hou, U. Farooq, J. Huang, K. Sun, R. Webster, H. Wu, Z. Chen, F. Yi, H. Song, X. Hao and J. Tang, *Adv. Funct. Mater.*, 2019, **29**, 1901720.
22 X. Chen, B. Che, Y. Zhao, S. Wang, H. Li, J. Gong, G. Chen, T. Chen, X. Xiao and J. Li, *Adv. Energy Mater.*, 2023, **13**, 2300391.
23 S. Yao, J. Wang, J. Cheng, L. Fu, F. Xie, Y. Zhang and L. Li, *ACS Appl. Mater. Interfaces*, 2020, **12**, 24112–24124.
24 J. Dong, Y. Liu, Z. Wang and Y. Zhang, *Nano Sel.*, 2021, **2**, 1818–1848.
25 X. Wang, R. Tang, C. Jiang, W. Lian, H. Ju, G. Jiang, Z. Li, C. Zhu and T. Chen, *Adv. Energy Mater.*, 2020, **10**, 2002341.
26 R. Nie and S. I. Seok, *Small Methods*, 2020, **4**, 1900698.
27 Y. Zhao, S. Wang, C. Jiang, C. Li, P. Xiao, R. Tang, J. Gong, G. Chen, T. Chen, J. Li and X. Xiao, *Adv. Energy Mater.*, 2022, **12**, 2103015.
28 X. Chen, X. Shu, J. Zhou, L. Wan, P. Xiao, Y. Fu, J. Ye, Y.-T. Huang, B. Yan, D. Xue, T. Chen, J. Chen, R. L. Z. Hoye and R. Zhou, *Light: Sci. Appl.*, 2024, **13**, 281.
29 M. Okil, A. Shaker, I. S. Ahmed, T. M. Abdolkader and M. S. Salem, *Sol. Energy Mater. Sol. Cells*, 2023, **253**, 112210.
30 C. Chen and J. Tang, *ACS Energy Lett.*, 2020, **5**, 2294–2304.
31 C. Battaglia, A. Cuevas and S. De Wolf, *Energy Environ. Sci.*, 2016, **9**, 1552–1576.

© 2025 The Author(s). Published by the Royal Society of Chemistry

Open Access Article. Published on 29 2025. Downloaded on 19.05.2026 16:14:10.
This article is licensed under a Creative Commons Attribution 3.0 Unported Licence.

32 Y. Cao, C. Liu, J. Jiang, X. Zhu, J. Zhou, J. Ni, J. Zhang, J. Pang, M. H. Rummeli, W. Zhou, H. Liu and G. Cuniberti, *Sol. RRL*, 2021, **5**, 2000800.
33 J. Li, J. Huang, K. Li, Y. Zeng, Y. Zhang, K. Sun, C. Yan, C. Xue, C. Chen, T. Chen, M. A. Green, J. Tang and X. Hao, *Sol. RRL*, 2021, **5**, 2000693.
34 X. Jin, Y. Fang, T. Salim, M. Feng, S. Hadke, S. W. Leow, T. C. Sum and L. H. Wong, *Adv. Funct. Mater.*, 2020, **30**, 2002887.
35 Y. Zhou, L. Wang, S. Chen, S. Qin, X. Liu, J. Chen, D.-J. Xue, M. Luo, Y. Cao, Y. Cheng, E. H. Sargent and J. Tang, *Nat. Photonics*, 2015, **9**, 409–415.
36 H. Zhou, J. Han, X. Pu and X. Li, *J. Materiomics*, 2021, **7**, 1074–1082.
37 U. A. Shah, S. Chen, G. M. G. Khalaf, Z. Jin and H. Song, *Adv. Funct. Mater.*, 2021, **31**, 2100265.
38 G. Liang, M. Chen, M. Ishaq, X. Li, R. Tang, Z. Zheng, Z. Su, P. Fan, X. Zhang and S. Chen, *Adv. Sci.*, 2022, **9**, e2105142.
39 A. Buyruk, D. Blätte, M. Günther, M. A. Scheel, N. F. Hartmann, M. Döblinger, A. Weis, A. Hartschuh, P. Müller-Buschbaum, T. Bein and T. Ameri, *ACS Appl. Mater. Interfaces*, 2021, **13**, 32894–32905.
40 J. Min, Z.-G. Zhang, Y. Hou, C. O. Ramirez Quiroz, T. Przybilla, C. Bronnbauer, F. Guo, K. Forberich, H. Azimi, T. Ameri, E. Spiecker, Y. Li and C. J. Brabec, *Chem. Mater.*, 2015, **27**, 227–234.
41 K. Kim, J. Han, S. Maruyama, M. Balaban and I. Jeon, *Sol. RRL*, 2021, **5**, 2000783.
42 X. Feng, X. Lv, J. Cao and Y. Tang, *ACS Appl. Mater. Interfaces*, 2022, **14**, 55538–55547.
43 G. Dennler, M. C. Scharber, T. Ameri, P. Denk, K. Forberich, C. Waldauf and C. J. Brabec, *Adv. Mater.*, 2008, **20**, 579–583.
44 S. Wang, Y. Zhao, B. Che, C. Li, X. Chen, R. Tang, J. Gong, X. Wang, G. Chen, T. Chen, J. Li and X. Xiao, *Adv. Mater.*, 2022, **34**, 2206242.
45 Y. Huang, R. Tang, G. Wang, G. Li, B. Che, Y. Wang, W. Lian, C. Zhu and T. Chen, *J. Mater. Chem. A*, 2022, **10**, 9892–9901.
46 G. Li, J. Dong, P. Xiao, B. Che, Y. Huang, Y. Zhang, R. Tang, C. Zhu and T. Chen, *Sci. China Mater.*, 2022, **65**, 3411–3417.
47 C. Nobre, A. Şen, L. Durão, I. Miranda, H. Pereira and M. Gonçalves, *Biomass Convers. Biorefin.*, 2023, **13**, 2267–2277.
48 Y. Huang, H. Gao, X. Peng, G. Wang, P. Xiao, B. Che, R. Tang, C. Zhu and T. Chen, *Sol. RRL*, 2023, **7**, 2201115.
49 J. Han, X. Pu, H. Zhou, Q. Cao, S. Wang, J. Yang, J. Zhao and X. Li, *J. Mater. Sci. Technol.*, 2021, **89**, 36–44.
50 Y. Huang, R. Tang, P. Xiao, B. Che, Y. Wang, H. Gao, G. Wang, C. Zhu and T. Chen, *ACS Appl. Mater. Interfaces*, 2022, **14**, 54822–54829.
51 E. M. Mkawi and Y. Al-Hadeethi, *Int. J. Energy Res.*, 2023, **2023**, 2636957.
52 Y. Zhang, S. Li, R. Tang, X. Wang, C. Chen, W. Lian, C. Zhu and T. Chen, *Energy Technol.*, 2018, **6**, 2126–2131.
53 J. Han, S. Wang, J. Yang, S. Guo, Q. Cao, H. Tang, X. Pu, B. Gao and X. Li, *ACS Appl. Mater. Interfaces*, 2020, **12**, 4970–4979.
54 Y. Itzhaik, O. Niitsoo, M. Page and G. Hodes, *J. Phys. Chem. C*, 2009, **113**, 4254–4256.
55 S. Nezu, G. Larramona, C. Choné, A. Jacob, B. Delatouche, D. Péré and C. Moisan, *J. Phys. Chem. C*, 2010, **114**, 6854–6859.
56 P. Reinhard, B. Bissig, F. Pianezzi, E. Avancini, H. Hagendorfer, D. Keller, P. Fuchs, M. Döbeli, C. Vigo, P. Crivelli, S. Nishiwaki, S. Buecheler and A. N. Tiwari, *Chem. Mater.*, 2015, **27**, 5755–5764.
57 F. Pianezzi, P. Reinhard, A. Chirilă, B. Bissig, S. Nishiwaki, S. Buecheler and A. N. Tiwari, *Phys. Chem. Chem. Phys.*, 2014, **16**, 8843–8851.
58 Y. Jiang, Y. Yang, L. Qiang, R. Fan, L. Li, T. Ye, Y. Na, Y. Shi and T. Luan, *Phys. Chem. Chem. Phys.*, 2015, **17**, 6778–6785.
59 M. Sutton, N. Robertson and T. Ameri, *J. Mater. Chem. A*, 2025, **13**, 17340–17349.

© 2025 The Author(s). Published by the Royal Society of Chemistry